Organic Electronics 13 (2012) 615–622

Contents lists available at SciVerse ScienceDirect

Organic Electronics

journal homepage: www.elsevier.com/locate/orgel

Light management in PCPDTBT:$PC_{70}BM$ solar cells: A comparison of standard and inverted device structures

Steve Albrecht [a], Sebastian Schäfer [a], Ilja Lange [a], Seyfullah Yilmaz [b], Ines Dumsch [b], Sybille Allard [b], Ullrich Scherf [b], Andreas Hertwig [c], Dieter Neher [a,*]

[a] Universität Potsdam, Institute of Physics and Astronomy, Soft Matter Physics, D-14476 Potsdam, Germany
[b] Bergische Universität Wuppertal, Macromolecular Chemistry and Institute for Polymer Technology, Gauss-Strasse 20, D-42097 Wuppertal, Germany
[c] Bundesanstalt für Materialwissenschaften (BAM), Unter den Eichen 44-46, D-12203 Berlin, Germany

ARTICLE INFO

Article history:
Received 25 October 2011
Received in revised form 13 December 2011
Accepted 28 December 2011
Available online 16 January 2012

Keywords:
Organic solar cells
Inverted solar cells
PCPDTBT
Low band-gap
Optical modeling

ABSTRACT

We compare standard and inverted bulk heterojunction solar cells composed of PCPDTBT:$PC_{70}BM$ blends. Inverted devices comprising 100 nm thick active layers exhibited short circuit currents of 15 mA/cm^2, 10% larger than in corresponding standard devices. Modeling of the optical field distribution in the different device stacks proved that this enhancement originates from an increased absorption of incident light in the active layer. Internal quantum efficiencies (IQEs) were obtained from the direct comparison of experimentally derived and modeled currents for different layer thicknesses, yielding IQEs of ~70% for a layer thickness of 100 nm. Simulations predict a significant increase of the light harvesting efficiency upon increasing the layer thickness to 270 nm. However, a continuous deterioration of the photovoltaic properties with layer thickness was measured for both device architectures, attributed to incomplete charge extraction. On the other hand, our optical modeling suggests that inverted devices based on PCPDTBT should be able to deliver high power conversion efficiencies (PCEs) of more than 7% provided that recombination losses can be reduced.

1. Introduction

The worldwide increasing demand for cheap electricity has triggered intense research on solar cells comprising organic semiconductors. Record values are currently achieved using soluble fullerene-derivatives as electron-acceptors and donor–acceptor-type co-polymers approaching and exceeding 8% efficiency [1–4]. The overall efficiency of planar solar cells is determined by several factors, one being the efficiency η_{abs} of the incident photons to be absorbed in the active layer under AM 1.5 illumination. Interference effects within the device structure cause η_{abs} to vary periodically with the thickness of the active layer. Efficient absorption is mostly realized in the 2nd absorption maximum, which is around 200–250 nm for many polymer:fullerene blends (with the optimum thickness primarily depending on the absorption properties, i.e. the long wavelength absorption onset of the active layer, see Supporting information Fig. S1).

Unfortunately, many highly efficient donor–acceptor-type co-polymers show significantly reduced fill factors (FFs) when increasing the active layer thickness. This is in contrast to the properties of the well known homopolymer poly(3-hexylthiophene) (P3HT) blended with fullerenes, where FFs exceeding 60% are measured even for blend thicknesses of up to 250 nm [5]. Optimized co-polymer devices, therefore, comprise active layers with thicknesses around the 1st absorption maximum, at 100 nm or even below [3,4,6,7], though increasing the layer thicknesses to the 2nd absorption maximum would allow a

* Corresponding author. Tel.: +49 (0) 331 977 1265; fax: +49 (0) 331 977 5615.
E-mail address: neher@uni-potsdam.de (D. Neher).

1566-1199/$ - see front matter © 2012 Elsevier B.V. All rights reserved.
doi:10.1016/j.orgel.2011.12.019

more complete absorption of the incident light. The overall reduction of device performance due to the drop in FF with increasing layer thickness has been attributed to inefficient charge-transport and collection. Therefore, alternative ways to increase the absorption while adjusting the active layer thickness to the 1st absorption maximum at around 100 nm need to be considered.

A smart strategy is to alter the optical field distribution within planar solar cell geometries [8], e.g. by the insertion of optical spacers [9,10] or by choosing different contact materials reducing parasitic absorptions and thereby increasing η_{abs} [11]. The most common device structure (here referred to as "standard") for organic solution processed solar cells is shown in Fig. 1a. The active layer is sandwiched between indium tin oxide (ITO) covered with poly(3,4ethylenedioxythiophene):poly(styrene sulfonate (PEDOT:PSS) and a low work function back electrode (Ca or Al) [4,12,13]. Inverted devices with metal-oxides like MoO_3 as hole- and TiO_2 or ZnO as electron-selective contacts have recently attracted attention because of their increased air stability compared to standard structures [14–17]. It was also shown that inverted architectures exhibits superior solar cell performance which was attributed to different absorption profiles, with reduced parasitic absorption in the PEDOT:PSS and the Ca layer [11,18]. Inverted structures are now widely used for high efficiency polymer:fullerene solar cells [15,16,19,20].

Poly[2,6-(4,4-bis(2-ethylhexyl)-4H-cyclopenta[2,1-b;3,4-b′]dithiophene)-alt-4,7-(2,1,3-benzothiadiazole)] (PCPDTBT) [21] has recently attracted considerable attention because of its low absorption band gap and high photovoltaic efficiency in blends with [6,6]-phenyl C_{71}-butyric acid methyl ester ($PC_{70}BM$). While initial studies performed on PCPDTBT:$PC_{70}BM$ processed in the standard geometry yielded a power conversion efficiency (PCE) of 3.2% [22], large improvements have been achieved by employing processing additives such as octanedithiol (ODT) and by using an inverted solar cell architecture [20,23]. However, to best of our knowledge, a comparative study of PCPDTBT:PCBM blends in standard and inverted cells has yet not been published.

Here we show that inverting the device structure of solar cells comprising a 100 nm spin-coated blend of PCPDTBT with $PC_{70}BM$ enhances the J_{sc} by 11%. Our experimental findings are rationalized by simulations of the optical field distributions within the multilayer structure with a transfer matrix formalism [8,24], which clearly illustrates an increase of the η_{abs} in the inverted device architecture. The comparison between the experimental short circuit current and the calculated η_{abs} allows the determination of the internal quantum efficiency (IQE) at simulated AM 1.5 simulation as a function of active layer thickness. We show that the IQE decreases continuously with thickness, pointing to inefficient charge carrier collection for thicker active layers.

2. Materials and methods

2.1. Solar cell fabrication

All solar cell devices were fabricated on structured ITO coated glass slides (Optrex) pre-cleaned in acetone, detergent, DI-water and isopropanol, and dried with a nitrogen gun. For standard devices, the pre-cleaned ITO substrates were plasma-cleaned and a 50–60 nm layer of PEDOT:PSS (Clevios AI 4083) was spin-cast on top. The samples were subsequently transferred into a nitrogen filled glove-box followed by annealing at 180 °C for 10 min. The active layer was spin-cast from solutions containing 1–3 blend ratios of PCPDTBT (M_w = 26,000 g/mol, PDI = 1.36, was prepared in a Stille type polycondensation following a procedure described in literature [21]) and $PC_{70}BM$ (99%, Solenne). Chlorobenzene was used as the solvent and 3 vol% diiodooctane (DIO) was added as a processing agent unless otherwise mentioned. Different layer thicknesses were attained by varying spin speed and blend concentration. Finally, 20 nm Ca and 100 nm Al were thermally evaporated with a base pressure below 10^{-6} mbar through shadow masks to define the active area to be 0.16 cm^2. For inverted devices a TiO_2 sol synthesized according to Ref. [9] was spin-cast at 5000 rpm onto ITO followed by heating to 80 °C for 10 min in air to form a TiO_2 layer with a thickness of 8–10 nm. Subsequently, the samples were transferred into the nitrogen-filled glove-box and heated to 140 °C for 10 min. After spin-coating the active layer, the devices

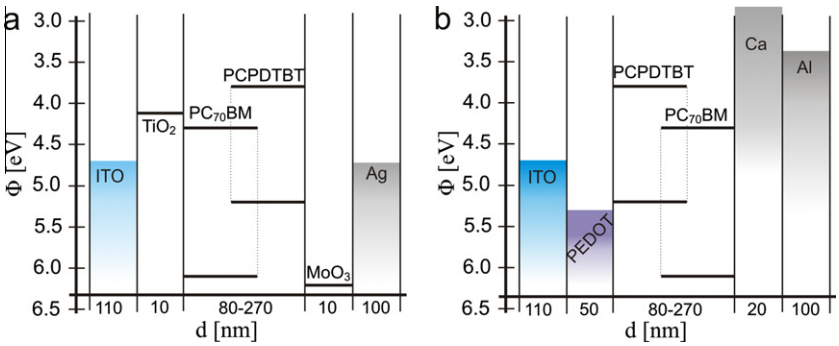

Fig. 1. Schematic device structure for (a) inverted and (b) standard device setup used in this work. The *x*-axes indicates the thickness range of each individual layer and the *y*-axes the work-functions measured with Kelvin Probe (in eV): ITO 4.7; PEDOT:PSS 5.3; Ca below 3; Al 3.3; TiO_2 4.1; MoO3 6.2 (for thicker films ~6.8); Ag 4.7. The values for HOMO and LUMO levels for the active layer were adopted from Refs. [6,35].

were completed by thermal evaporation of 10 nm of MoO_3 and 100 nm of Ag. Due to the high boiling point of DIO, all solar cells have been dried in vacuum at room-temperature for at least 5 h prior to evaporation of the back contact, since residual DIO functions as a hole trap [25].

2.2. Determination of optical constants and layer thickness

The optical constants of the metal oxides and the PEDOT:PSS were derived from transmission and reflection measurements on the respective materials on glass slides with a Varian Cary 5000 spectrophotometer equipped with an integrating sphere. Within the system air/film/substrate/air, the film thickness as well as the optical constants of the substrate and its thickness needs to be known. The optical constants of the film have been iteratively fitted point by point with the Newton–Raphson-method until the measured and theoretical reflection and transmission data converged [26]. The optical constants of the PCPDTBT:PC_{70}BM blend were deduced from spectroscopic ellipsometry of the blend layer on crystalline silicon (100) substrates by means of a M2000DI rotating compensator ellipsometer (J.A. Woollam Co.). The analysis was performed with the WVASE software (3.740). Due to the complex absorption spectrum of the blend, the generalized oscillator model employed 11 Gaussian absorption peaks between 1.5 and 6.1 eV center wavelengths. The surface roughness was implied with a 8 nm thick EMA (50% void) roughness layer. A MSE of only 3.5 shows the high accuracy of the fit. The optical constants of Ca, Al and ITO as well as Ag have been taken from literature [8,27,28]. Thicknesses have been measured with surface profilometry (Dektak 3, Veeco) for the active layer and via absorption on quartz glass substrates for the thin TiO_2 layers.

2.3. Determining the electrode work functions

The work functions have been determined via Kelvin Probe measurements as described in a recent publication [29], using highly ordered pyrolytic graphite (HOPG) as reference (work function of 4.6 eV [30]). Estimates of the work functions of all electrodes employed in our solar cells were obtained by performing measurements on the following samples: 100 nm of Ag or Al thermally evaporated on glass-slides, 10 nm of MoO_3 on Ag, 20 nm of Ca on Al, untreated ITO, 10 nm thick TiO_2 on ITO as well as 50 nm PEDOT:PSS on ITO.

2.4. External quantum efficiency (EQE)

The EQE was measured with monochromated light from tungsten lamp mechanically shopped to 140 Hz for detection with a lock-in amplifier. The intensity of the lamp was checked with an UV enhanced crystalline solar cell calibrated at Newport before each measurement. The quality of the EQE setup was cross checked with a KG3 filtered crystalline silicon reference solar cell calibrated at Fraunhofer ISE.

2.5. Solar cell characteristics

J–V characteristics were measured under illumination with an Oriel class A simulator calibrated to 100 mW/cm^2. The samples were temperature controlled to 20 °C during measurement. The calibration of the sun simulator was done with a KG3 filtered silicon reference cell calibrated at Fraunhofer ISE. All shown data (except in the Supporting information) are corrected for spectral mismatch (mismatch factor for PCPDTBT:PC_{70}BM $M = 0.95$) according to [31].

2.6. Optical modeling

The simulation of the solar cell short circuit currents have been performed by modeling the absorption of the active layer in the device stack with the transfer matrix formalism [8,24]. Comparison of the fraction of absorbed light with the measured EQE spectra at short circuit conditions yielded the internal quantum efficiency as a function of wavelength. Reflectivity spectra were measured for each cell to confirm the accuracy of the determination of the optical constants as described above.

3. Results and discussion

Fig. 1 summarizes the solar cell architectures of the studied solar cells. In the standard device configuration as shown in Fig. 1b, the active layer is sandwiched between PEDOT:PSS and Ca covered with Al. For the inverted devices the active layer is embedded between the electron selective TiO_2 and the hole selective MoO_3 contacts (Fig. 1a). Fig. 1 also shows the work functions of the different contacts as determined via Kelvin Probe measurements. The work function values are quite comparable to literature data for TiO_2 [7], MoO_3 [32] and PEDOT:PSS Clevios AI4083 [33]. We found that high FFs in the inverted geometry are only achieved with very thin TiO_2 layers (8–10 nm) while FF decreases drastically when the TiO_2 thickness of increases beyond 20 nm (see Supporting information S2). By applying 15 min UV-exposure with a Benda UV-hand-lamp to the solar cell the FF can be partially recovered even for thicker TiO_2 films, indicating that the UV-exposure promotes the trap filling thereby improving the electrical conductivity of the TiO_2 [34].

Fig. 2(a) shows the measured EQE of a standard and an inverted solar cell with a PCPDTBT:PC_{70}BM blend layer thickness of 100 nm. Clearly, the inverted device exhibits a higher EQE throughout the measured wavelength range. Accordingly, the J_{sc} of the inverted device is more than 10% higher compared to the standard structure (see Fig. 4).

Comparison of the EQE and the corresponding modeled fraction of absorbed light in the active layer for the different geometries shows that the external quantum efficiency scales well with the modeled absorption. We, actually find that the internal quantum efficiency as calculated from the EQE and the fraction of absorbed photons is rather similar for both device structures, with a mean value of about 71%. This implies that the higher EQE for inverted devices stems mainly from the higher absorption of the active layer. Also,

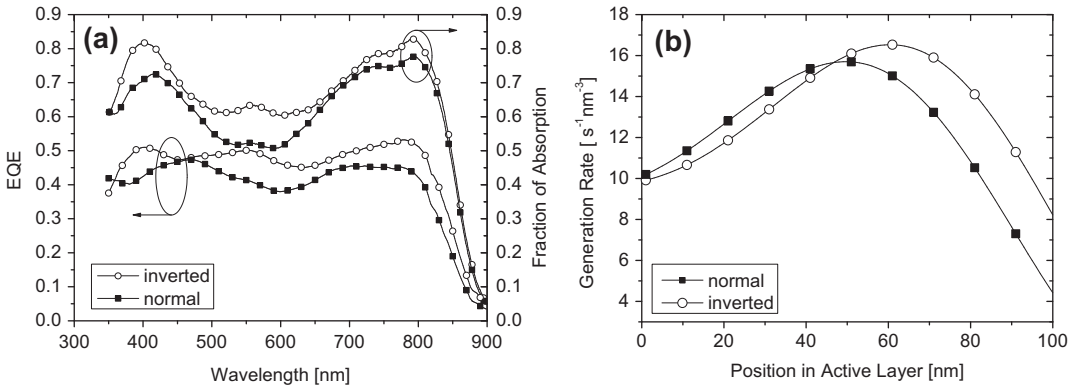

Fig. 2. (a) EQE and modeled fraction of absorbed light $A(\lambda)$ in standard and inverted devices with an active layer thickness of 100 nm. (b) Modeled exciton generation rate in the active layer as a function of position within the active layer of inverted (open circles) and standard devices (filled squares).

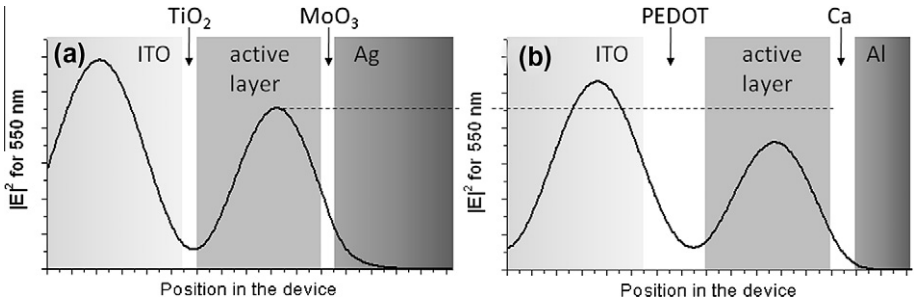

Fig. 3. Modulus squared of the optical electric field (normalized to the incoming plane wave) in the device stack for (a) inverted devices and (b) standard devices for 550 nm with the same *y*-axes scale-bar.

the variation of the IQE with wavelength is rather weak (Fig. 3) and a systematic difference in IQE for wavelength-ranges where the polymer or the PCBM absorption is dominant as reported by Burkhard et al. [36] has not been found. The high quality of the modeled absorption in the device stack is shown by the very good agreement between the modeled and measured reflectivity of the full device (Fig. S5).

According to Petersson et al. [24], the energy dissipation Q_{act} in the active layer at position x is given by

$$Q_{act}(x,\lambda) = \frac{1}{2} c\varepsilon_0 \alpha n |E(x,\lambda)|^2 \quad (1)$$

Evidently, Q_{act} is proportional to the refractive index n and the absorption coefficient α of the active layer as well as the modulus squared of the optical electric field $|E(x,\lambda)|^2$ normalized to the incoming field. Knowing the power of the incoming AM 1.5 spectrum, the exciton generate rate $g(x)$ can be calculated by dividing $Q_{act}(x,\lambda)$ by the energy of a single photon at wavelength λ and integrating over the wavelength range determined by the transmission through the ITO (λ_{begin}) and absorption onset of the active layer (λ_{end}) [8,37].

$$g(x) = \int_{\lambda_{begin}}^{\lambda_{end}} \frac{\lambda}{hc} Q_{act}(x,\lambda) d\lambda \quad (2)$$

In Eq. (2) the photon to exciton conversion efficiency is assumed to be one meaning that every single photon absorbed in the active layer initially creates an exciton. The exciton generation rate versus position in the active layer is shown in Fig. 2(b) for standard and inverted devices with a nominal active layer thickness of 100 nm. The main difference is a shift of the generation profile towards the back-electrode. Interestingly, the rate for excited state formation near the back electrode is considerably larger for the inverted cell geometry, which accounts in part for the higher J_{sc} of this device.

The normalized modulus of the optical electric field is shown in Fig. 3 for inverted (a) and standard devices (b) with an active layer thickness of 100 nm for a wavelength of 550 nm. This wavelength has been chosen as the difference in EQE and absorption between the two device stacks is most prominent at 550 nm. Inversion of the layer structure causes a slight shift of the maximum of the electric field towards the back electrode but mainly increases the overall modulus throughout the whole active layer.

It has been reported that introducing optical spacers between the active layer and the back electrode in standard devices [9] or matching the refractive index of the front-contact to ITO [7] increases J_{sc}. Systematical optical modeling studies (data not shown) for the inverted structure of our PCPDTBT:PC$_{70}$BM blends showed that decreasing the MoO$_3$ thickness actually increases J_{sc} meaning that the MoO$_3$ layer inserted between the active material and the metallic Ag contact does primarily not function as an optical spacer, and that the inverted structure is already well

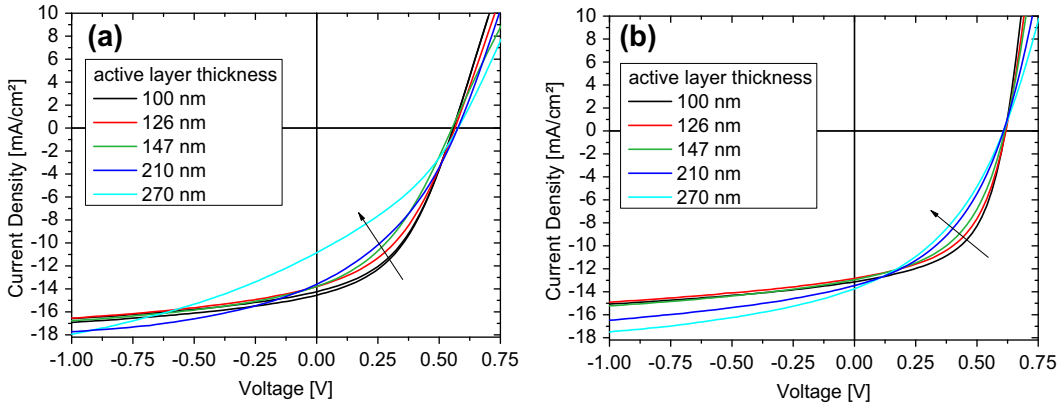

Fig. 4. *J–V* characteristics of devices with different active layer thickness in (a) inverted and (b) standard device structure. All characteristics were measured under simulated AM 1.5G illumination calibrated to 100 mW/cm^2 and corrected for spectral mismatch.

optimized with a thin MoO_3 film [38]. Increasing the MoO_3 thickness moves the maximum of the modulus squared of the optical electric field closer to the back contact, resulting in a reduced exciton generation rate. Also, decreasing the refractive index of the TiO_2 in the simulation caused J_{sc} to increase. According to our simulations, further improvement of light absorption in the active region for a blend thickness of 100 nm can only be achieved when applying light trapping mechanisms, which is beyond the scope of this paper.

In the next step, a systematic variation of the active layer thickness was performed. Fig. 4 shows the resulting *J–V* characteristics under simulated AM 1.5G spectra at 100 mW/cm^2 for inverted (a) and standard (b) devices, with active layer thicknesses between 100 and 270 nm. The photovoltaic parameters derived from these curves are summarized in Fig. 5.

For both device architectures, the device performance declines with layer thickness, but the effect is more pronounced for the inverted structure. This decrease is in part due to a continuous decrease of the FF with thickness. Also, the measured short-circuit currents derivate largely from the prediction by optical modeling (using a constant internal quantum efficiency of 68%) at high layer thickness. In particular, we find that J_{sc} is higher for the inverted structure for a layer thickness smaller than ca. 170 nm, while it drops considerably below the value for the standard device architecture for high thicknesses. This is in contrast to optical modeling which predict J_{sc} of the inverted device to be 9–15% higher for all thicknesses, with a maximum difference at around 175 nm. Poor fill factors and low short circuit currents have been attributed to either a field-dependent efficiency of free carrier generation or to recombination losses. In the former case, the photocurrent will scale with the internal electric field, which is not the case in our devices (see Fig. S3). Also, regular and inverted devices exhibit different fill factors for the same layer thickness (having almost the same open circuit voltage), ruling out field-dependent generation as the main process governing the photocurrent characteristics. This is in accordance with recent findings by Jamieson et al. [39]. Alternatively, low fill factor of PCPDTBT:fullerene solar cells have been explained by significant, possible trap-assisted, recombination [22,40,41]. Recently, Bailey et al. presented a detailed study on the interrelation between blend morphology, carrier transport and photovoltaic properties of a blend of a related polymer, poly[N-9″-hepta-decanyl-2,7-carbazole-*alt*-5,5-(4′,7′-di-2-thienyl-2′,1′,3′-benzothiadiazole)] (PCDTBT), with $PC_{70}BM$ [42]. These authors concluded that the decrease in device performance with layer thickness is due to trap-assisted recombination in presence of a broad distribution of holes traps, and that deep traps are caused by the rather low structural order in these blends. It was also suggested that recombination losses decrease with increasing inverse bias.

Therefore, to evidently show that inverting the device structure improves light absorption for all layer thicknesses, we have compared the light-generated current at the most negative bias of −1 V to the absorption efficiency $\eta_{abs}^{blend}d$ which is the fraction of incident photons absorbed in the active layer, accounting for the spectral irradiance $I(\lambda)$ of the AM 1.5G illumination integrated over the wavelength-range of the blend absorption.

$$\eta_{abs}^{blend}(d) = \frac{\int_{350\ nm}^{900\ nm} \lambda \cdot A(\lambda, d) \cdot I(\lambda) d\lambda}{\int_{350\ nm}^{900\ nm} \lambda \cdot I(\lambda) d\lambda} \quad (3)$$

In Eq. (3), $A(\lambda, d)$ is the fraction of light absorbed in the active layer at a given wavelength λ and thickness d. The comparison is shown in Fig. 6(a). In accordance with the prediction by optical modeling, the photocurrent of the inverted device at −1 V exceeds the current of the corresponding regular structure for all layer thicknesses. Also, the reverse-bias currents are largest at a layer thickness of 270 nm, which complies with the predicted behavior. Finally, IQEs calculated from the photocurrents at −1 V are well comparable for both devices for a given thickness (Fig. 6(b)), meaning that the efficiency for converting an absorbed photon into a free carrier is independent of device architecture.

We finally, like to address the poorer fill factor and short circuit current in the inverted device. Following the arguments outlined above, the balance between extraction and recombination of free charge carriers must be more

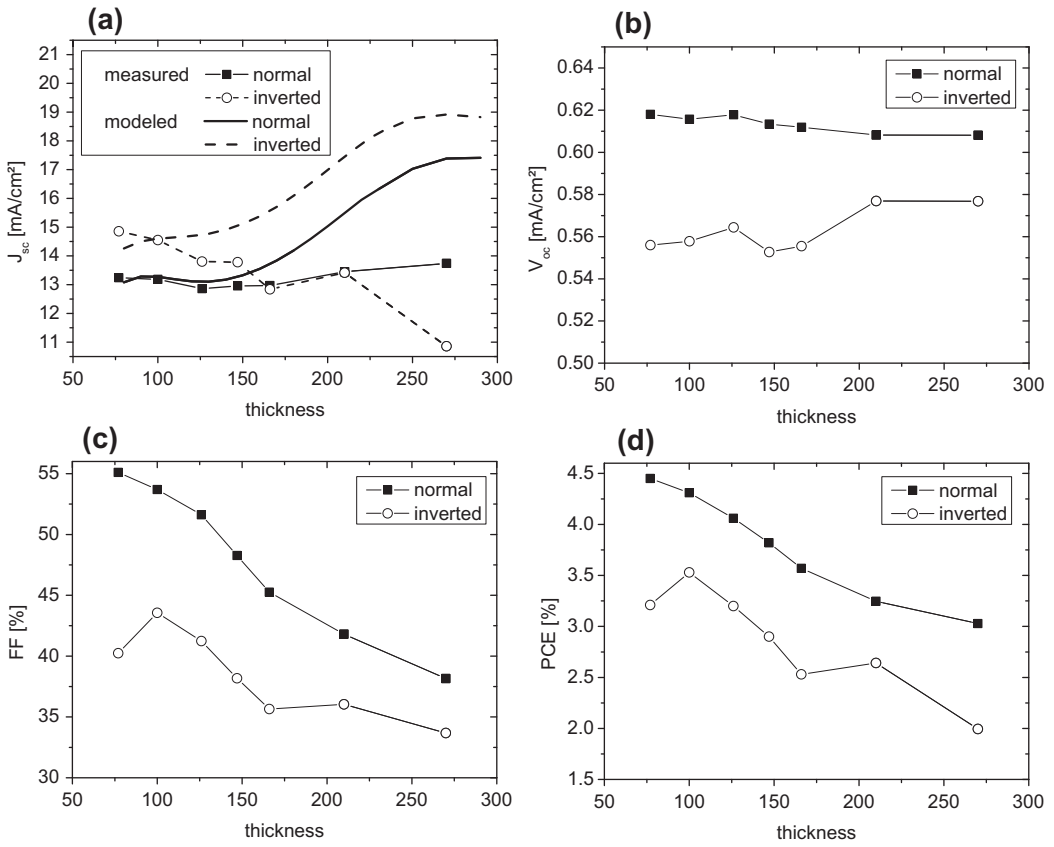

Fig. 5. (a) Measured J_{sc} from simulated AM 1.5G at 100 mW/cm^2 corrected for spectral mismatch for inverted (dashed line + open circles) and standard cells (solid line + filled squares), plotted together with modeled short circuit current under the assumption of a constant IQE of 68% for inverted (dashed black line) and standard cells (solid black line), (b) measured open circuit voltages, (c) measured fill factors, (d) measured power conversion efficiency.

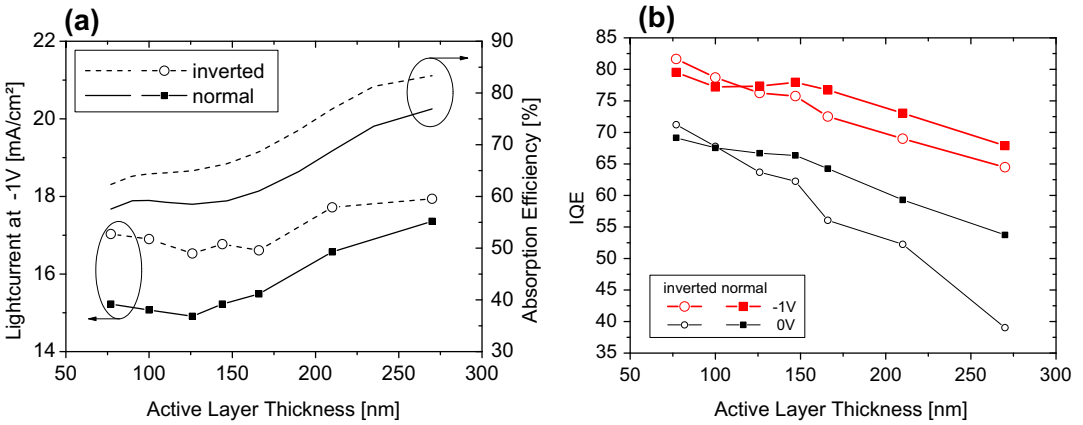

Fig. 6. (a) Comparison of the current under illumination of AM 1.5G irradiance with 100 mW/cm^2 at −1 V and the absorption efficiency of the blends in the wavelength range between 350 and 900 nm, (b) internal quantum efficiency for different layer thicknesses, calculated from measured (under AM 1.5G with 100 mW/cm^2) currents at 0 V (black) and −1 V (red) and the modeled fraction of absorption in the active layer for inverted (open circles) and standard devices (filled squares). (For interpretation of the references to colour in this figure legend, the reader is referred to the web version of this article.)

unfavorable in the inverted device. Holes have been found to be the slower carriers in PCPDTBT:$PC_{70}BM$ blends [43]. As shown in Fig. 7, the generation profile seen from the hole-extracting contact is rather different for both types of devices. In particular, the path length for hole extraction is remarkably higher in the inverted device with a thick active layer compared the standard structure. This in turn might increase the amount of holes occupying traps and concurrently enforce trap-assisted recombination. In addition, the PCPDTBT phase was shown to undergo slow

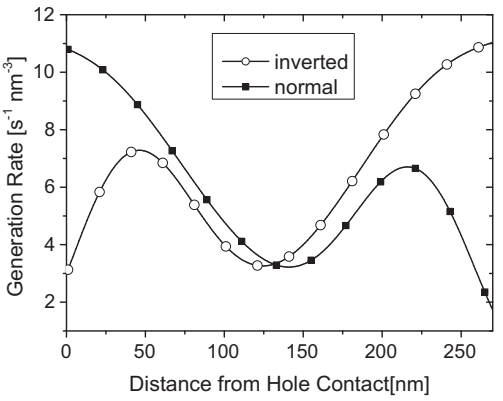

Fig. 7. Simulated exciton generation profile versus distance from the hole selective contact for normal (filled squares) and inverted (open circles) devices with an active layer thickness of 270 nm.

drying in presence of the additive, which can promote segregation of the hole-transporting PCPDTBT towards the bottom contact. Agostellini et al. reported a pronounced vertical composition profile in PCPDTBT:PCBM blends processed with the additive [41]. Such segregation might aggravate the collection of holes at the top contact in the inverted device structures. Note that weak segregation will have an only minor affect on the optical field profile. In fact, we find very good agreement between the modeled and measured reflectance on ITO/TiO_2-substrates when assuming that the optical constants are homogeneous throughout the entire layer. Evidently, the lower fill factors and power conversion efficiencies of our inverted devices must be related to more pronounced recombination losses, caused either by vertical phase segregation or different path length of hole extraction in the two types of devices. Here it is important to note that inverted devices comprising a 140 nm thick annealed P3HT:PCBM blend layer exhibited very high FFs and a Voc equal to the standard structure (see Supporting information S2), even in absence of UV exposure. Annealed P3HT:PCBM layers were shown to have reduced coefficients for bimolecular recombination, which is probably related to the high structural and electronic order in this particular blend system [44–46].

4. Conclusion

In summary, we have shown that inverted device stacks comprising a 100 nm thick bulk heterojunction composed of PCPDTBT and $PC_{70}BM$ show 11% larger short circuit currents compared to the standard device structure. Optical modeling of the optical field distribution in the different device stacks proves that this enhancement originates from an increased absorption of incident light in the active layer. The internal quantum efficiency for both architectures was found to be ~70% for a layer thickness of 100 nm, but it decreased continuously with layer thickness. The simultaneous deterioration of the FF for increasing thickness indicates that charge collection becomes increasingly inefficient for thicker blend layers, probably caused by strong mono- or bimolecular recombination. On the other hand, our optical simulations show that inverted solar cells based on PCPDTBT:$PC_{70}BM$ are capable of delivering high efficiencies at larger active layer thicknesses, provided that recombination losses can be suppressed. Noticeably, a J_{sc} of 19.0 mA/cm^2 is predicted for a moderate internal quantum efficiency of 70% and a layer thicknesses around 270 nm. Assuming a V_{oc} of 0. 61 V and a FF of 62%, a PCE of more than 7% should be achievable for the inverted device structure. Further work will, therefore, be devoted to the understanding and reduction of extraction losses in these blends.

Acknowledgements

S.A. acknowledges Dr. Basudev Pradhan and Ulrike Schreiber for the help with the TiO_2 synthesis and Dr. James Blakesley for the modification of the optical modeling software. This work was funded by the Bundesministerium für Bildung und Forschung (BMBF) within the PVcomB project (FKZ 03IS2151D).

Appendix A. Supplementary data

Supplementary data associated with this article can be found, in the online version, at doi:10.1016/j.orgel.2011.12.019.

References

[1] Konarka Press Release, 2010.
[2] Solarmer Press Release, 2010.
[3] T.-Y. Chu, J. Lu, S. Beaupré, et al., J. Am. Chem. Soc. 133 (2011) 4250.
[4] Y.Y. Liang, Z. Xu, J.B. Xia, et al., Adv. Mater. 22 (2010) E135.
[5] C.J. Brabec, S. Gowrisanker, J.J.M. Halls, et al., Adv. Mater. 22 (2010) 3839.
[6] M.C. Scharber, M. Koppe, J. Gao, et al., Adv. Mater. 22 (2010) 367.
[7] Y. Sun, C.J. Takacs, S.R. Cowan, et al., Adv. Mater. 23 (2011) 2226.
[8] G.F. Burkhard, E.T. Hoke, M.D. McGehee, Adv. Mater. 22 (2010) 3293.
[9] S.H. Park, A. Roy, S. Beaupre, et al., Nat. Photonics 3 (2009) 297.
[10] R. Schueppel, R. Timmreck, N. Allinger, et al., J. Appl. Phys. 107 (2010) 6.
[11] A. Hadipour, D. Cheyns, P. Heremans, et al., Adv. Energy Mater. 1 (2011) 930.
[12] R.C. Coffin, J. Peet, J. Rogers, et al., Nat. Chem. 1 (2009) 657.
[13] C. Piliego, T.W. Holcombe, J.D. Douglas, et al., J. Am. Chem. Soc. 132 (2010) 7595.
[14] C. Waldauf, M. Morana, P. Denk, et al., Appl. Phys. Lett. 89 (2006) 3.
[15] Y.-J. Cheng, C.-H. Hsieh, Y. He, et al., J. Am. Chem. Soc. 132 (2010) 17381.
[16] Y.M. Sun, J.H. Seo, C.J. Takacs, et al., Adv. Mater. 23 (2011) 1679.
[17] C.-Y. Li, T.-C. Wen, T.-H. Lee, et al., J. Mater. Chem. 19 (2009) 1643.
[18] T. Ameri, G. Dennler, C. Waldauf, et al., J. Appl. Phys. 103 (2008) 6.
[19] C.M. Amb, S. Chen, K.R. Graham, et al., J. Am. Chem. Soc. 133 (2011) 10062.
[20] M. Morana, H. Azimi, G. Dennler, et al., Adv. Funct. Mater. 20 (2010) 1180.
[21] Z. Zhu, D. Waller, R. Gaudiana, et al., Macromolecules 40 (2007) 1981.
[22] D. Mühlbacher, M. Scharber, M. Morana, et al., Adv. Mater. 18 (2006) 2884.
[23] J. Peet, J.Y. Kim, N.E. Coates, et al., Nat. Mater. 6 (2007) 497.
[24] L.A.A. Pettersson, L.S. Roman, O. Inganas, J. Appl. Phys. 86 (1999) 487.
[25] S. Cho, J.K. Lee, J.S. Moon, et al., Org. Electron. 9 (2008) 1107.
[26] K. Peter, Diploma Thesis, University of Konstanz, 1993.
[27] C.M. Ramsdale, N.C. Greenham, J. Phys. D: Appl. Phys. 36 (2003) L29.
[28] E. Palik, Handbook of Optical Constants of Solids, vol. 1, Academic Press Limited, 1995.
[29] I. Lange, J.C. Blakesley, J. Frisch, et al., Phys. Rev. Lett. 106 (2011) 216402.

[30] M.M. Beerbom, B. Lägel, A.J. Cascio, et al., J. Electron Spectrosc. 152 (2006) 12.
[31] V. Shrotriya, G. Li, Y. Yao, et al., Adv. Funct. Mater. 16 (2006) 2016.
[32] M. Kroger, S. Hamwi, J. Meyer, et al., Appl. Phys. Lett. 95 (2009) 3.
[33] S. Kirchmeyer, A. Elschner, K. Reuter, Pedot: Principles and Applications of an Intrinsically Conductive Polymer, Taylor and Francis Group, 2011.
[34] S. Sista, M.H. Park, Z.R. Hong, et al., Adv. Mater. 22 (2010) 380.
[35] H.-Y. Chen, J. Hou, S. Zhang, et al., Nat. Photon 3 (2009) 649.
[36] G.F. Burkhard, E.T. Hoke, S.R. Scully, et al., Nano Lett. 9 (2009) 4037.
[37] D.W. Sievers, V. Shrotriya, Y. Yang, J. Appl. Phys. 100 (2006) 7.
[38] T.-Y. Chu, S. Alem, P.G. Verly, et al., Appl. Phys. Lett. 95 (2009) 063304.
[39] F.C. Jamieson, T. Agostinelli, H. Azimi, et al., J. Phys. Chem. Lett. 1 (2010) 3306.
[40] M. Morana, M. Wegscheider, A. Bonanni, et al., Adv. Funct. Mater. 18 (2008) 1757.
[41] T. Agostinelli, T.A.M. Ferenczi, E. Pires, et al., J. Polym. Sci. Part B: Polym. Phys. 49 (2011) 717.
[42] Z.M. Beiley, E.T. Hoke, R. Noriega, et al., Adv. Energy Mater. 1 (2011) 954.
[43] M. Lenes, M. Morana, C.J. Brabec, et al., Adv. Funct. Mater. 19 (2009) 1106.
[44] A. Pivrikas, G. Juska, A.J. Mozer, et al., Phys. Rev. Lett. 94 (2005).
[45] I.A. Howard, R. Mauer, M. Meister, et al., J. Am. Chem. Soc. 132 (2010) 14866.
[46] J. Kniepert, M. Schubert, J.C. Blakesley, et al., J. Phys. Chem. Lett. 2 (2011) 700.